International Journal of Mass Spectrometry 291 (2010) 1–12

Contents lists available at ScienceDirect

International Journal of Mass Spectrometry

journal homepage: www.elsevier.com/locate/ijms

Designing multi-field linear time-of-flight mass spectrometers with higher-order space focusing

Murat Yildirim[a,*], Omer Sise[b], Mevlut Dogan[b], Hamdi S. Kilic[a]

[a] Department of Physics, Science Faculty, Selcuk University, 42075 Konya, Turkey
[b] Department of Physics, Science and Arts Faculty, Afyon Kocatepe University, 03200 Afyonkarahisar, Turkey

ARTICLE INFO

Article history:
Received 8 July 2009
Received in revised form
22 December 2009
Accepted 24 December 2009
Available online 14 January 2010

PACS:
82.80.Rt
07.75.th

Keywords:
Wiley and McLaren
Time-of-flight mass spectrometer
Space focusing
Mass resolution
SIMION

ABSTRACT

In this paper we present numerical modelling results for linear time-of-flight mass spectrometers (TOFMSs) with higher-order space focusing. A brief account of the TOFMS theory is given together with optimal geometries and electric fields which provide space focusing condition (i.e. the zero variation in ion time-of-flight caused by a change in initial position). The effect of the initial velocity distribution, a dominating factor that restricts resolution in TOFMSs, on the time-width of a peak in the mass spectrum was demonstrated. The results have shown that the limitations of the mass resolution by different initial velocities of the ions play a significant role in determining the order of space focusing required in practice. At room temperature no significant improvement in the mass resolution can be expected by increasing the order of space focus, because the time spread due to the velocity dispersion and "turn-around" time of the ion with a mass of 100 amu is about ~20 ns. Therefore, the optimum resolving power is about $m/\Delta m = 200$, which is also experimentally measured using a homemade TOFMS. Nevertheless, the theoretical analysis of the space focusing (no thermal energy distribution) is necessary as it provides a reference for judging the importance of velocity distributions, as deviations from the ideal case.

1. Introduction

Time-of-flight mass spectrometer (TOFMS) is one of the simplest mass analyzing devices, which separates ions, after their initial acceleration by uniform electric fields, according to their velocities when they drift in a free-field region. It can be a simpler technology for mass analysis compared to scanning analyzers such as magnetic sectors, quadrupoles and ion traps, and can readily reach mass resolving power ($m/\Delta m$) of 1000–10000 with very high efficiency by the use of simple, homogeneous accelerating fields in ion sources [1–3]. In combination with matrix-assisted laser desorption/ionization (MALDI), it has paved the way for new applications for biomolecules and polymers [4,5].

A major drawback with TOFMS has been the relatively poor mass resolution due to the spread in the initial thermal energies or velocity of the ions with the same mass-to-charge (m/z) ratio as well as the spatial distribution of them within the ionization region. It is possible to minimize the degradation in resolution brought about by the initial distributions. To minimize the effects of velocity distribution on time resolution, several methods were successfully introduced, such as delayed pulsed extraction [6], reflectrons [7], electrostatic sectors [8,9], orthogonal acceleration [10], and multi-turn ion optical geometries [11].

The time differences resulting from the spatial distribution of the ions along the axis of the flight tube is commonly minimized by incorporating the two-field acceleration geometry and space-focusing principles introduced by Wiley and McLaren [6]. The focus condition given by Wiley and McLaren makes the flight time of ions independent of their generating points in the ionization region. Improvements to the Wiley–McLaren space focusing have been proposed by a number of authors [12–17]. These articles make reference to providing second- or higher-order corrections to Wiley–McLaren space focusing. The equations of motion for space focusing are commonly solved by assuming that the extracted ions have no initial velocity. However, in a *real* laboratory TOFMS, the velocity of the ion beam will exist in a Maxwellian distribution corresponding to the temperature of the ion beam. The existence of this velocity distribution will result in degraded resolution. At room temperature (300 K or 26 meV) no significant improvement in the mass resolution can be expected by increasing the order of space focus from first- to higher-order because of the time spread due to the velocity dispersion and "turn-around" time of the ions. Therefore, the optimum resolving power is limited to $m/\Delta m$~200.

* Corresponding author.
E-mail address: muratyildirim@selcuk.edu.tr (M. Yildirim).

1387-3806/$ – see front matter © 2010 Elsevier B.V. All rights reserved.
doi:10.1016/j.ijms.2009.12.014

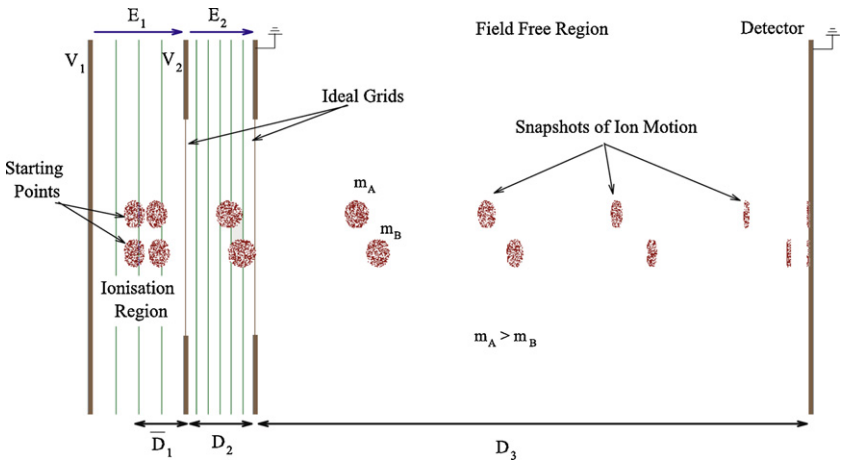

Fig. 1. Simulation of a two-field linear TOFMS with space focusing: identical ions formed at slightly different distances (s) from the center of the source region ($\bar{D}_1$) shall have the same flight time. The ion source electrodes were assumed to have centered holes with a diameter of 10 mm covered with a perfect grid (realistic grids were not included in the simulations because their effects strongly depend on the type of grids used). The ionization region is located in the middle of the first and second plate, the molecular beam axis coming from the axis, and the ionizing radiation being perpendicular to the figure plane. At a defined moment in time, $t = 0$, a packet of ions that was generated in the source is accelerated to a fixed kinetic energy, and released in the field-free drift region. The flight times of ions are recorded and used to calculate m/z.

Even and Dick [15] have reported $m/\Delta m = 1200$ using a three-field linear TOFMS with second-order focusing. But, they used the pulsed extraction technique which gives the higher resolution.

In this paper, we describe the design of multi-field linear TOFMSs, considering the analysis of the equations of motion for higher space focusing. The effects of initial velocities on the time-dispersion of ions are demonstrated numerically using SIMION[18]. It is shown that the higher-order space focusing with multi-field device is not realized due mainly to dispersion in initial thermal velocity of the ions. This was experimentally checked using a home-made three-field linear TOFMS without using pulsed extraction and velocity focusing techniques. By measuring the time-of-flight spectra of a sample molecule, CO, the spectrometer gives a low resolution of about 200.

2. Theory of TOFMS

Likely the simplest strategy for determining the ion mass-to-charge ratio is time-of-flight mass spectrometry in which ions are accelerated to high kinetic energies by well-defined DC potentials, and their subsequent travel times across a length of field-free region are measured and used to determine m/z values (see Fig. 1). The laser (or electron) beam used in the ionization source has a finite spatial beam width. This width along with the atomic/molecular beam width from the nozzle jet expansion results in ions being created in the interaction region at different positions. The positions of these ions are randomly distributed with this region, a given ion being located D_1 from the end of the region as shown. A voltage on one of the grids creates an electric field E_1 by the potential V_1 and V_2 on the first and the second plate which causes the positively charged ions to move into the acceleration regions. There, a high electric field E_2 causes the ions to accelerate so that they pass into the long, field free drift region. Ions with different mass-to-charge ratios will have attained different velocities when entering the drift region and thus will arrive at the ion detector at different times since their speed is proportional to the inverse square root of m/z.

In a multi-field linear TOFMS, the total flight time of an ion T_m (a sum of times the particle spent in different regions of the TOFMS), its terminal velocities v_i, and the final ion energy E_f (if it is assumed that ions are generated at the middle of the ionization region with zero initial energy) are simply given in the following equations [17]:

$$T_m = \frac{\upsilon_1 - u_0}{a_1} + \sum_{i=2}^{m} \frac{\upsilon_i - \upsilon_{i-1}}{a_i} + \frac{D_{m+1}}{\upsilon_m} \tag{1}$$

$$\upsilon_m = \left(u_0^2 + \sum_{i=1}^{m} 2a_i D_i \right)^{1/2} \tag{2}$$

$$E_f = q \sum_{i=1}^{m} D_i E_i \tag{3}$$

where u_0 is the initial velocity component of the ion, q is the ion charge, a_i is the acceleration produced by the electric field E_i, and m is the number of the fields. D_{m+1} is the length of the field-free region, and $\bar{D}_1$ here is the distance to the center of the source while D_1 is the relative coordinate in the ionization region ($D_1 = \bar{D}_1$ for the middle of the ionization region). According to Eq. (1) both D_1 and u_0 will affect T_m. Thus ions with the same m/z can have different flight times depending on where and with which kinetic energy they are formed. The result will be peaks in the TOF spectrum whose shapes are influenced by these parameters.

The ability of the instrument to compensate for initial formation volume is called space resolution $\mathcal{R}_s$. In conventional TOFMSs, space resolution is maximized by selecting ion drawout and acceleration fields which satisfy the focus condition $d^n T_m / dD_1^n = 0$. Setting the derivatives of T_m with respect to D_1 to zero one can obtain after some straightforward algebra [17]:

$$2K_m \left[\frac{1}{R_m} + K_m^{n-1/2} \left(1 - \frac{1}{R_2} \right) + \sum_{i=2}^{m-1} \left(\frac{K_m}{K_i} \right)^{n-1/2} \left(\frac{1}{R_i} - \frac{1}{R_{i+1}} \right) \right] - (2n-1)L_{m+1} = 0 \tag{4}$$

$$K_m = \sum_{j=2}^{m} (1 + R_j L_j) \tag{5}$$

where we set $u_0 = 0$. Here, $L_i = D_i/D_1$ and $R_i = E_i/E_1$ ($i = 2, 3, \ldots, m$) are dimensionless parameters. In this relation, n rep-

resents the order of space focus required. The space resolution is then described as [17]:

$$\mathcal{R}_s = \frac{T(\bar{D}_1)}{2\Delta T_s} \tag{6}$$

where ΔT_s is the base width.

The initial velocity distribution of the ions will also contribute to the overall resolution. When two ions with the same m/z ratio are initially moving in opposite directions, towards and away from the detector, a time spread ΔT_{u_0} occurs due to the turn-around time of the ion, which is given by [17]:

$$\Delta T_{u_0} = \frac{2u_0}{a_1}. \tag{7}$$

This time spread can be corrected by using time-lag focusing [6], and cannot be corrected by a reflectron, even though it originates from a velocity spread.

Finally, the mass resolving power of a TOFMS, $\mathcal{R}_m = m/\Delta m$, can be calculated by two ways:

$$\mathcal{R}_m = m\frac{\Delta T_m}{\Delta T_{1/2}} \tag{8}$$

$$\mathcal{R}_m = \frac{T(\bar{D}_1)}{2\Delta T_{1/2}} \tag{9}$$

where m is the mass of an ion, ΔT_m is the time separation for adjacent masses $(T_{m+1} - T_m)$, $T(\bar{D}_1)$ is the ion's flight time, and $\Delta T_{1/2}$ is the full width at half maximum of the ion's peak in the time-of-flight spectrum. The attainable resolution of a TOFMS is limited, particularly at higher mass. As m increases, ΔT_m becomes progressively smaller and more difficult to differentiate. The above equations relate the mass resolution of the spectrometer to the time resolution. This is extremely useful since the time is the quantity that is actually experimentally measured.

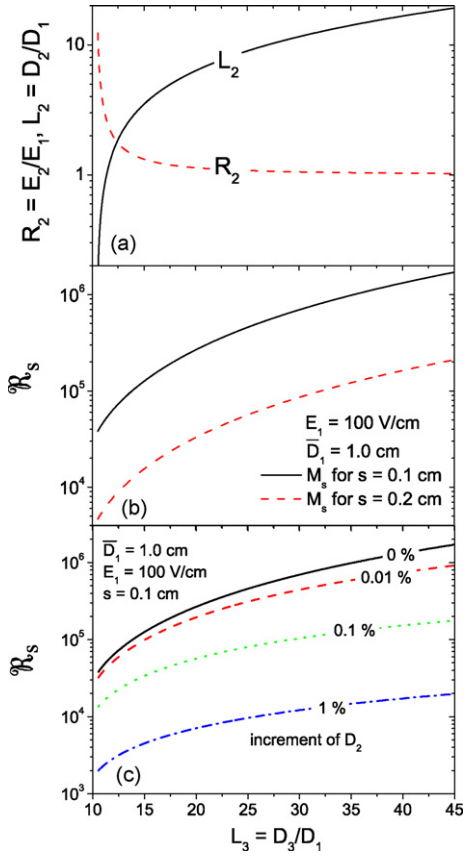

Fig. 2. (a) Second-order solutions for the dimensionless quantities R_2 and L_2 and (b) space resolution $\mathcal{R}_s$ in the two-field device as a function of L_3. The space resolution has been calculated for all the systems with $\bar{D}_1 = 1.0$ cm, $E_1 = 100$ V/cm, and interaction region sizes of $s = 0.1$ and 0.2 cm. Second-order focusing only occurs under geometrically restricted circumstances. (c) Comparison of the space resolutions for second-order space focusing with a small increment in D_2 value.

Table 1
The result of space resolution calculations for three different two-field TOFMS cases (see Fig. 3). The space resolution $\mathcal{R}_s$ is determined from the time of flights for ions starting different positions with zero initial energy within the interaction region. Other parameters are $m = 100$ amu, $s = \pm 0.1$ cm, $\bar{D}_1 = 1$ cm, $E_1 = 100.00$ V/cm.

	L_3	L_2	R_2	$T(\bar{D}_1)$/μs	ΔT_s/ns	$\mathcal{R}_s$
(a)	12	1.500	2.000	6.483	0.05	0.7×10^5
(b)	16	4.094	1.257	7.786	0.03	1.3×10^5
(c)	20	6.337	1.135	8.839	0.01	4.4×10^5

Now, the problem is finding the mechanical and electrical arrangements which provide the best time resolution and the best spatial focusing. One can find the solution using either analytical or numerical methods. Both of solutions can in principle be useful to define the direction of the investigations. But, analytical solution for $u_0 \neq 0$ is not simple because of the complexity of the ion directions. Therefore, it is better to solve the equations of motion numerically for initial velocity distributions. We used ion optics ray-tracing simulation program SIMION 8.0 [18], which is the main program used in mass spectroscopy (for some recent examples see Refs. [19–24]). By using the representative initial conditions, the program is also able to model the statistical ion distributions (e.g. Gaussian and Normal).

To estimate the space resolution obtainable, we assumed that the laser produced ions with an initial start-position distribution described by a one-dimensional Gaussian distribution centered on the axis at the interaction region (the contribution of these factors is essentially Gaussian in nature [4]). The applied voltages to the grids were obtained from the analytical solutions for space focusing conditions. The next step is to project them forward in time to simulate their trajectories in the flight tube towards the detector. Ion–ion Coulomb repulsion was not taken into consideration in these simulations. All SIMION simulations were performed at a calculation level of TQual$\geq +10$, and the geometry files were produced using a resolution of 10 points per millimeter for better accuracy [25]. Two simplifying assumptions were also made in these calculations, that the vacuum was good and so no ion-neutral collisions occurred during the flight (see Ref. [26] for ion motion differences between vacuum and viscous environments) and that there were no magnetic field imperfections in the drift region to disturb the ion motion.

Table 2
The results of mass resolution calculations for three different two-field TOFMS cases. The mass resolving power $\mathcal{R}_m$ is determined from the individual peak width (full width at half maximum) for beam temperatures of 1 μK, 1 mK, and 1 K, respectively.

	L_3	u_0	ΔT_m/ns	$\Delta T_{1/2}$/ns	$\mathcal{R}_m$
(a)	12	1 μK	32.0	0.002	1.60×10^6
		1 mK	32.0	0.052	6.15×10^4
		1 K	32.0	1.523	2.10×10^3
(b)	16	1 μK	38.8	0.002	2.44×10^6
		1 mK	38.8	0.045	8.53×10^4
		1 K	38.8	1.595	2.44×10^3
(c)	20	1 μK	44.1	0.002	2.60×10^6
		1 mK	44.1	0.050	8.80×10^4
		1 K	44.1	1.535	2.87×10^3

3. Results and discussion

3.1. Two-field first-order space focusing

Although the basic operation of the two-field time-of-flight mass spectrometer has been well described in the literature [12,14], it will be reviewed here briefly so that the derivation of the first- and second-order focusing condition may be better understood. A more complete description can be found in Ref. [17].

A schematic representation of a two-field TOFMS was presented in Fig. 1. This instrument has a two-grid ion source with a flight tube. Using Eq. (1), the flight-time of any ion having a known initial position and velocity can be calculated. Particular distributions of initial ion positions and velocities in the source lead to a distribution of ion arrival-times at the detector, and ultimately to a simulated TOFMS peak shape. Ions that travel farthest in the source region will have the highest energy and velocity, but be the last to leave the source. These ions catch up to the slower ions at the space-

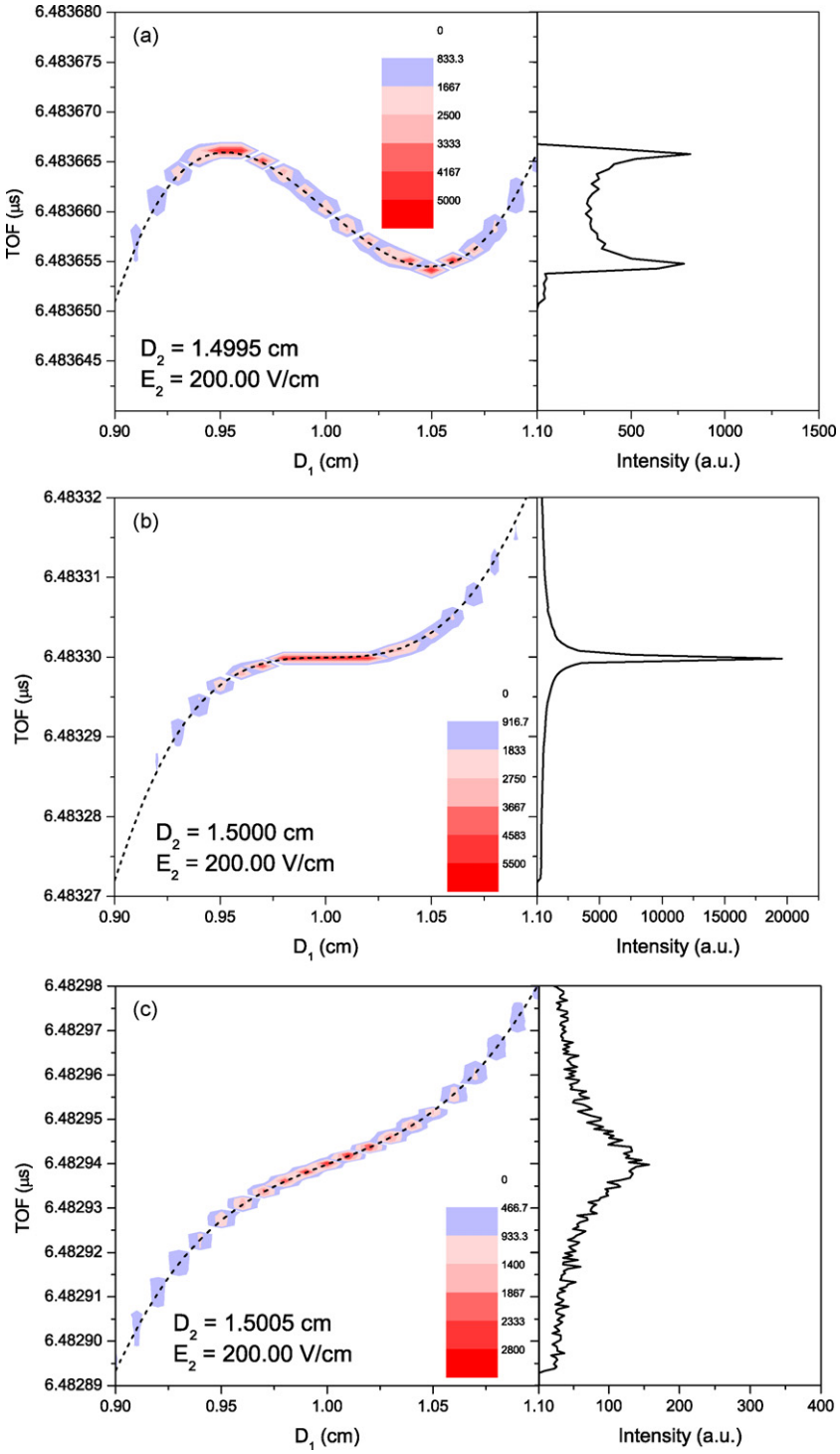

Fig. 3. Flight times distributions as a function of the distance travelled in the ionization region for a two-field TOFMS for an ion of mass 100 amu and charge +1e. The extraction and acceleration fields are 100.00 and 200.00 V/cm, the lengths of the acceleration region and flight tube are 1.5 and 16 cm, and the source region is 0.2 cm. If D_2 value in (b) is varied by a small amount (−0.0005 cm in (a) or +0.0005 cm in (c)) the time dispersion curve is altered.

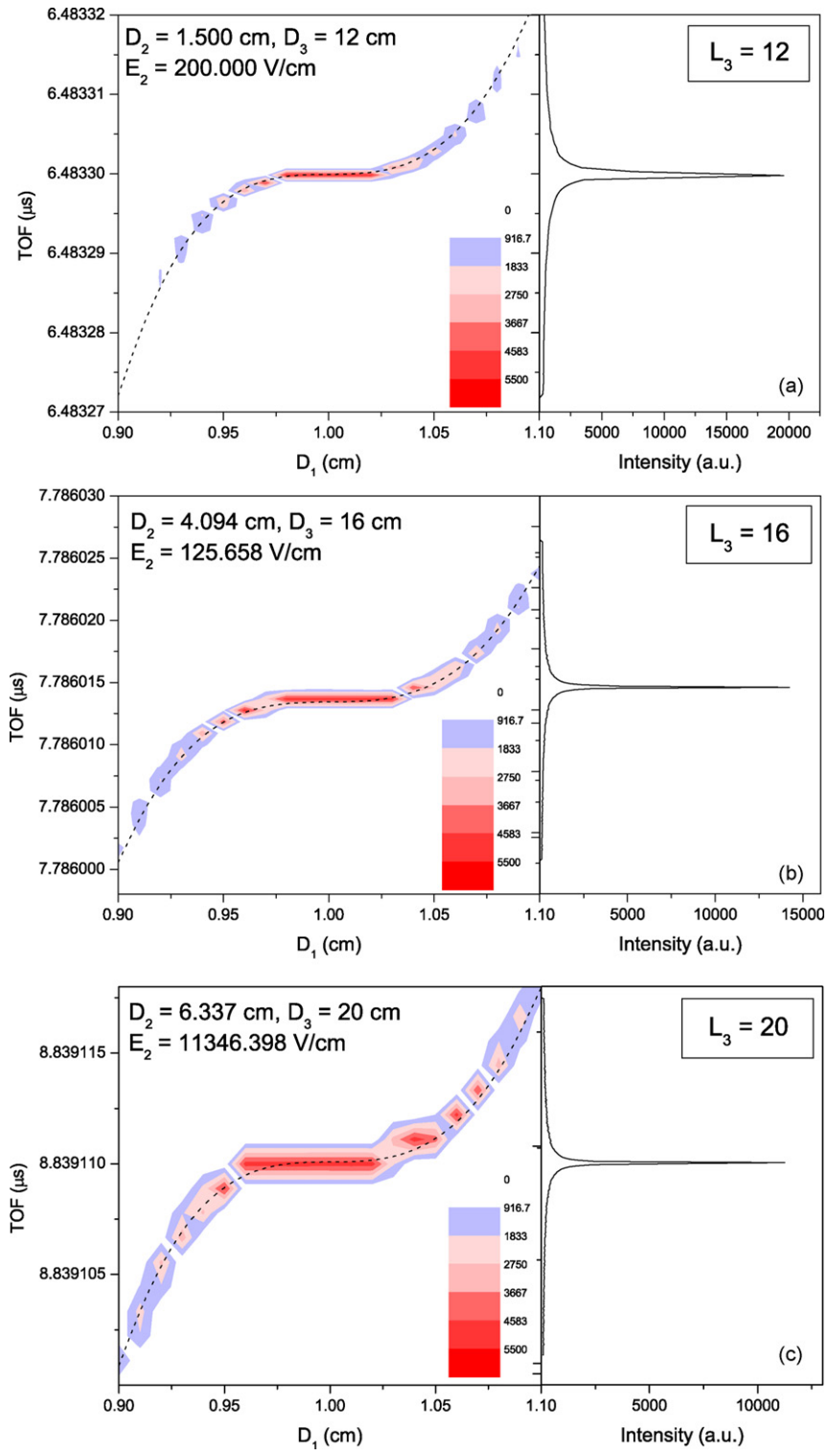

Fig. 4. Flight times distributions as a function of the distance travelled in the ionization region for three two-field TOFMSs with (a) $L_3 = 12$, (b) 16, and (c) 20, for an ion of mass 100 amu and charge +1e. The extraction field is 100.00 V/cm and $\bar{D}_1 = 1$ cm. D_2, D_3, and E_2 are indicated in the figure.

focus plane. The distance of this space-focus plane from the source is a function of the potentials applied to the first and second grids. When the space-focus plane is not located at the detector surface, distortion of peak shapes can be expected. Experimentally, a non-optimal setting of the ion focus voltage is observed as a loss of peak height and a broadening of the peak.

For a two-field TOFMS ($m = 2$) first-order space focus ($n = 1$) is achieved by setting the first derivative to zero $dT_m/dD_1 = 0$. From Eq. (4), one can obtain the well known formula for the length of the flight tube of a two-field TOFMS at the first-order space focusing plane [17]:

$$L_3 = 2K_2^{3/2}\left[1 - \frac{L_2}{K_2^{1/2} + K_2}\right] \tag{10}$$

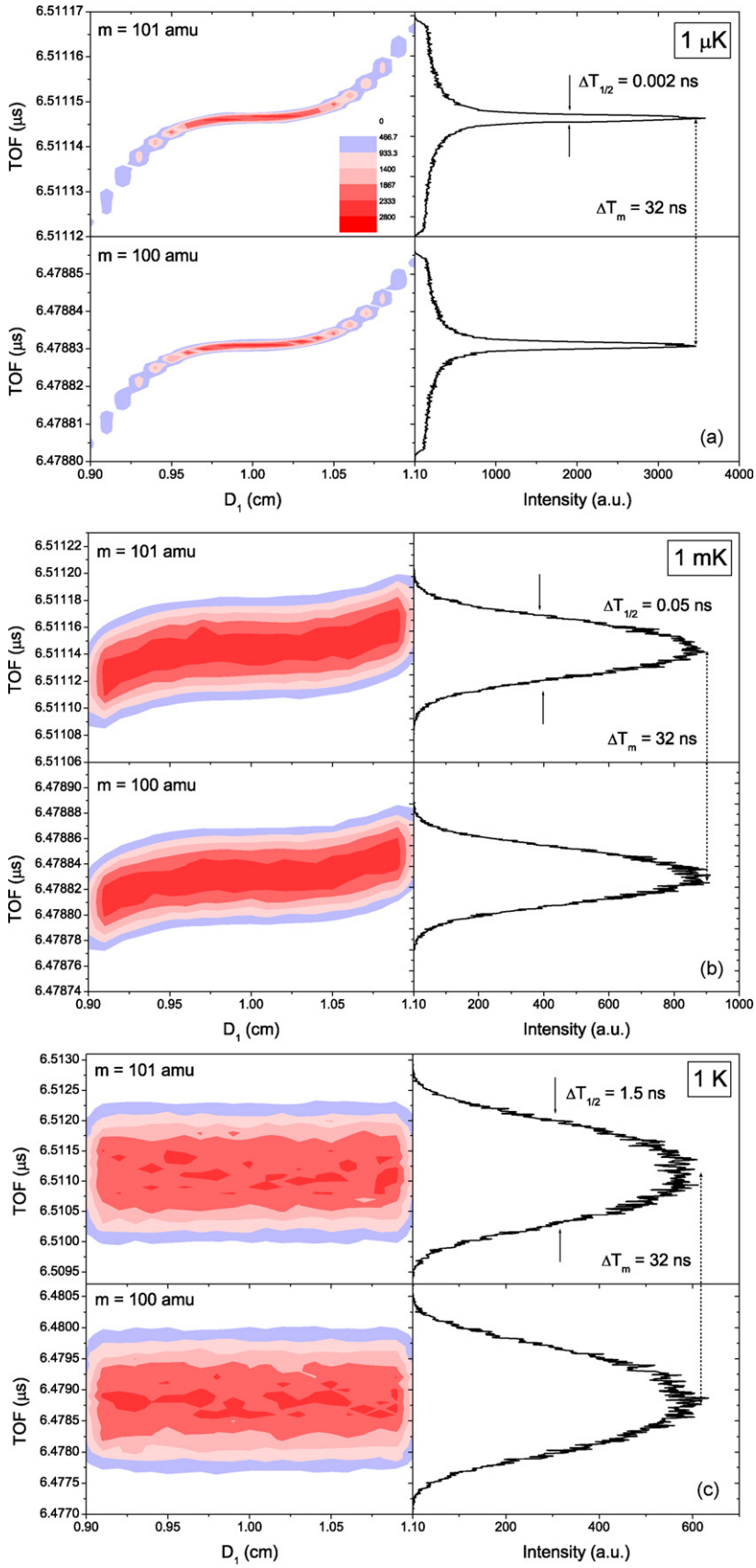

Fig. 5. Simulated time-of-flight spectra of the ions with 100 and 101 amu for a two-field TOFMS with $L_3 = 12$ for three different beam temperatures: (a) 1 μK, (b) 1 mK, and (c) 1 K. The intensities of the peaks supposed to be not exact as it plays no significant role. The $\Delta T_{1/2}$ value is determined by entering the values describing the left and right edges of the peak at FWHM.

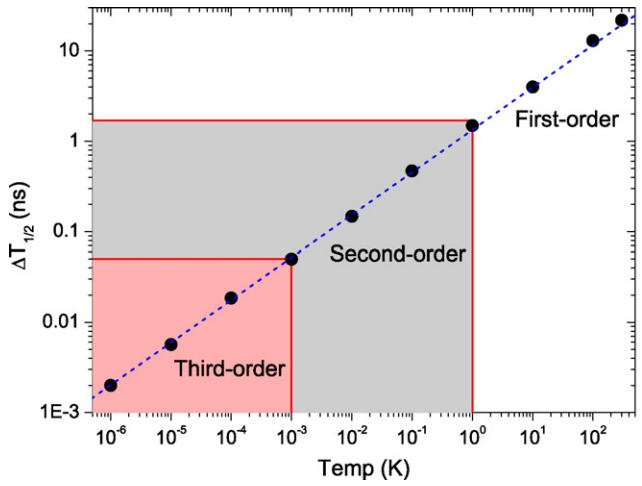

Fig. 6. $\Delta T_{1/2}$ is plotted as a function of beam temperature for a two-field TOFMS with $L_3 = 12$.

where $K_2 = 1 + R_2L_2$, $L_2 = D_2/D_1$, $L_3 = D_3/D_1$, and $R_2 = E_2/E_1$. Therefore, if D_1, D_2, and D_3 are fixed values, then the first-order space focusing condition is satisfied by a unique value of $R_2 = E_2/E_1$, which can be determined by Eq. (10). In the practical application of this equation one would choose the dimensions and adjust the fields to obtain maximum resolution by monitoring the minimum widths of the TOF peaks. This kind of spectrometer is used in numerous experiments up to date, e.g. with gas cells or molecular beams, and achieves high mass resolutions.

3.2. Two-field second-order space focusing

Second-order space focus is achieved by setting both dT_m/dD_1 and d^2T_m/dD_1^2 to zero. Using dimensionless parameters in the derivatives of time-of-flight in a two-field design one can obtain two simultaneous equations. These equations can be solved keeping $R_2L_2 = K_2 - 1$ (> 2) as a free parameter, giving L_2 and L_3 in a useful functional form [17]:

$$L_2 = \frac{D_2}{D_1} = \frac{K_2^{1/2}(K_2^{1/2}+1)(K_2-3)}{K_2 + K_2^{1/2} - 2} \tag{11}$$

$$L_3 = \frac{D_3}{D_1} = \frac{2(K_2^{3/2}+K_2^2)}{K_2 + K_2^{1/2} - 2}. \tag{12}$$

In Fig. 2(a) and (b), second-order solutions for the dimensionless quantities R_2 and L_2 and space resolution $\mathcal{R}_s$ are plotted as a function of L_3. It is clear that ΔT_s is minimized by using optimal E_i and minimum s/D_1 consistent with the requirements of the focus condition. Since space focusing condition does not rely on the absolute magnitudes on E_1 and E_2 but on their ratio R_2, it is possible to use large values of the acceleration fields and still maintain the focusing condition. In practice, E_1 should be as high as possible, because higher electric fields help to reduce the arrival time spread arising from initial velocity distribution and usually improve detection efficiency.

The representation of space focusing conditions allows one to read off values for the required electric field and dimension to satisfy space focusing for an overall length of the flight tube. In this way, one can design a TOFMS having a smaller size and weight that is particularly attractive to outer space instrumentation applications. It can be seen that there was a noticeable increase in space resolution as the length of the flight tube also increased. Therefore, the resolution of TOFMS depends to a large extent on the length of the flight tube. To obtain good measuring conditions and good mass resolutions, the flight tube must be as long as possible. However, due to practical limitations, the field-free region in conventional TOFMS cannot be longer than a few meters (1–2 m).

In Fig. 2(c), calculations show that the space resolution is noticeably deteriorated by violation of the length of the electrodes. For each geometry, the optimum distance D_2 satisfied the second-order condition was increased by 0.01%, 0.1%, and 1%. If there is only a 1% error in L_2, the resolution is reduced by about an order of magnitude and the benefit of second-order space focusing is lost, which is in agreement with the previous results [15–17]. Therefore, care should be taken in the accurate machining of the electrodes of TOFMS, especially of reducing surface distortions in the vertical direction.

In Fig. 3, we calculated the time dispersion curve as a function of initial ion position (D_1) for an ion of mass 100 amu and charge +1e for the optimum acceleration field. Using the parameters given in Fig. 2(a) for $L_3 = 12$, the time dispersion curve and time-of-flight spectra were calculated, where the extraction field E_1 was fixed to 100.00 V/cm, and the length of the acceleration region and flight tube were 1.5 and 16 cm, respectively. The source region in this case is 0.2 cm wide ($s = \pm 0.1$ cm) and the middle of the source is located with a $\bar{D}_1$ of 1 cm. As can be seen in Fig. 3(b), where $D_2 = 1.5000$ cm and $E_2 = 200.00$ V/cm are the optimal values, the space focusing condition is fulfilled. However, if D_2 value is varied by a small amount (± 0.0005 cm) the time dispersion curve is

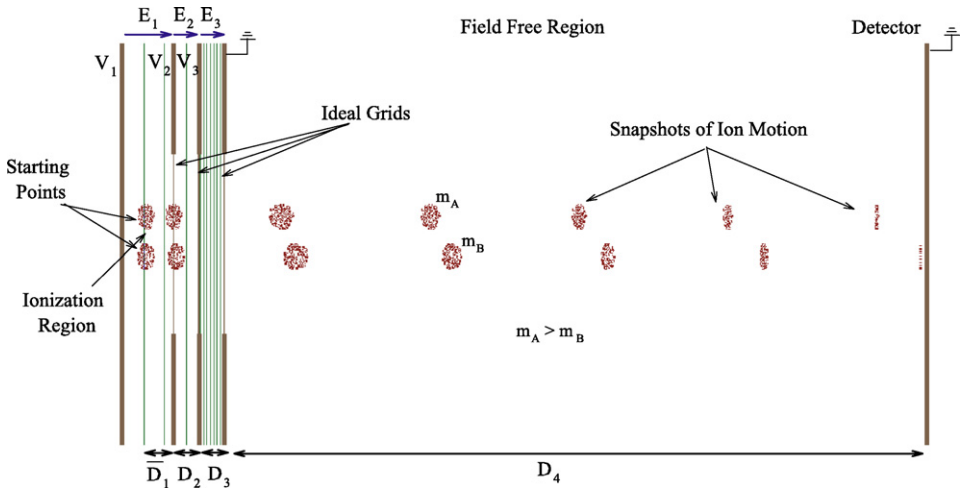

Fig. 7. Three-field TOFMS with $D_1 = D_2 = D_3$.

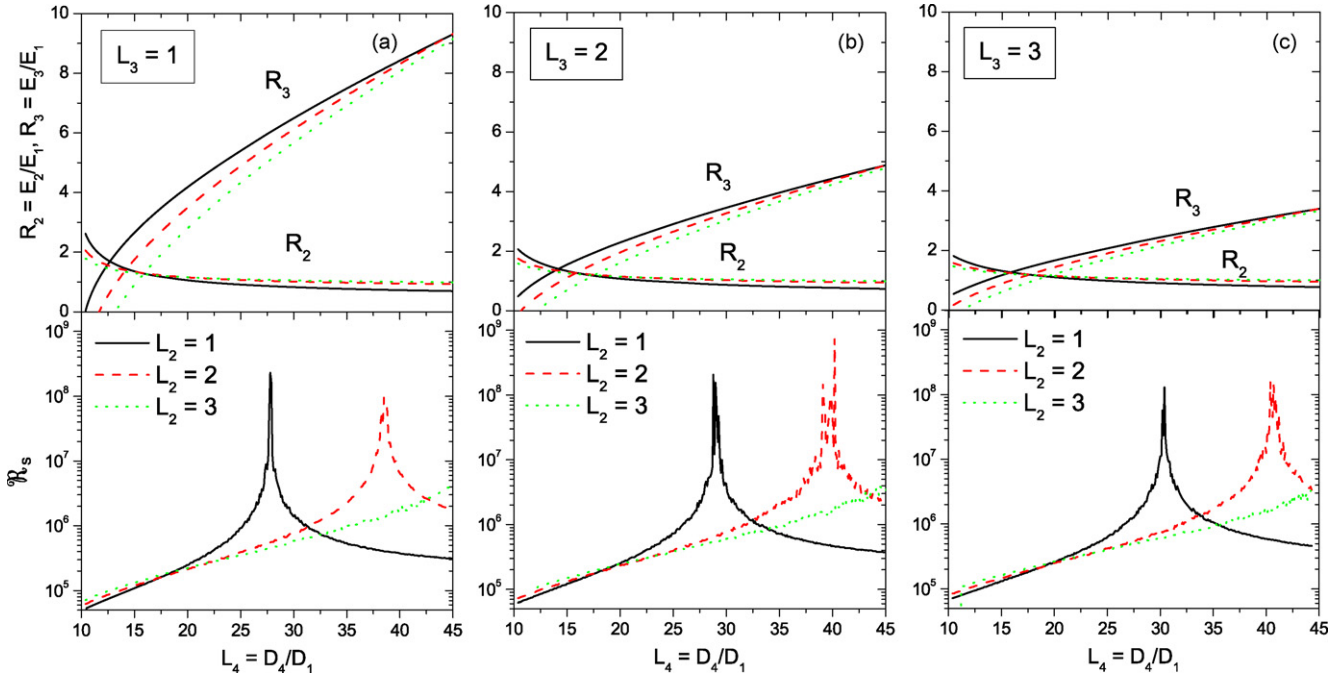

Fig. 8. Second-order solutions with three-field TOFMS and calculated space resolution $\mathcal{R}_s$ as a function of L_4 for selected values of L_2 and L_3. For the TOFMS with three acceleration regions the optimized design parameters are functions of two auxiliary parameters R_2 and R_3. The improved resolution is the result of a third-order space focusing.

altered. The same curve alteration was also observed for slightly different electric fields (200.05 and 199.95 V/cm). Therefore, the space resolution is highly affected by the errors resulted from uncorrected geometries and wrong applied voltages.

The arrival time versus the ion initial position (D_1) for three different two-field TOFMSs with $L_3 = 12$, 16 and 20 are shown in Fig. 4. In Table 1, the space focus width (ΔT_s) and space resolution ($\mathcal{R}_s$) were calculated for each geometry with an interaction size of $s = \pm 0.1$ cm. To further assess the resolution of the TOFMS, peak simulations were performed using a Monte-Carlo type approach in which both the initial position and velocity were randomly sampled. The ions have a distribution of initial velocities u_0 according to the beam temperature which also contributes to line broadening. A maximum number of 100,000 ions was found to give adequate statistics. Fig. 5 shows the flight time distributions for the masses 100 and 101 and the corresponding time resolution. Ions are assumed to be spread over a 0.2 cm wide and the beam temperature considered here is 1 μK, 1 mK, and 1 K, respectively.

Using flight times and peak widths from a TOF spectrum, a value of the mass resolution can be deduced using Eq. (9). For a two-field TOFMS with $L_3 = 12$ and 1 K beam temperature, this equation delivers a value of $\mathcal{R}_m = 2161$ for mass 100 with the simulated values of $T_m = 6.483\ \mu$ s and $\Delta T_{1/2} = 1.5$ ns. Calculated mass resolving powers due to the axial velocity distribution for three two-field TOFMSs are listed in Table 2.

Finally, $\Delta T_{1/2}$ is plotted in Fig. 6 as a function of beam temperature for a two-field TOFMS with $L_3 = 12$. It is clearly seen that the performance of TOFMS with higher-order space focusing is limited by the initial velocity characteristics of the ion beam.

Table 4
The results of mass resolution calculations for three different three-field TOFMS cases. The mass resolving power $\mathcal{R}_m$ is determined from the individual peak width (full width at half maximum) for beam temperatures of 1 μK, 1 mK, and 1 K, respectively.

	L_4	u_0	ΔT_m/ns	$\Delta T_{1/2}$/ns	$\mathcal{R}_m$
(a)	16	1 μK	36.9	0.003	1.44×10^6
		1 mK	36.9	0.045	8.18×10^4
		1 K	36.9	1.504	2.45×10^3
(b)	28	1 μK	47.6	0.001	3.19×10^6
		1 mK	47.6	0.045	1.05×10^5
		1 K	47.6	1.480	3.22×10^3
(c)	40	1 μK	57.0	0.002	3.57×10^6
		1 mK	57.0	0.045	1.27×10^5
		1 K	57.0	1.479	3.85×10^3

3.3. Three-field second-order space focusing

Three-field linear TOFMS has the advantage that it would be easier to configure than a two-field device if second-order space focusing is required. Higher resolution can be accomplished with third-order space focusing if specific operational conditions (¡1 mK) are observed. Fig. 7 shows, schematically, the three-field linear TOFMS. Since there is no constraint on the mechanical dimensions, the solutions R_2 and R_3 for the second-order focusing are presented graphically in Fig. 8 for selected values of L_2 and L_3 as a function of L_4. There exists an optimum in each case, and the configuration of electrodes and electric fields for some L_4 provides the best resolution. It is clear that this improved resolution is the result

Table 3
The result of space resolution calculations for three different three-field TOFMS cases with $L_2 = L_3 = 1$ (see Fig. 9). The space resolution $\mathcal{R}_s$ is determined from the time of flights for ions starting different positions with zero initial energy within the interaction region. $m = 100$ amu, $s = \pm 0.1$ cm, $\bar{D}_1 = 1$ cm, $E_1 = 100.00$ V/cm.

	L_4	L_3	L_2	R_2	R_3	$T(\bar{D}_1)$/μs	ΔT_s/ns	$\mathcal{R}_s$
(a)	16	1	1	1.277	2.999	7.411	0.0293	1.3×10^5
(b)	28	1	1	0.859	6.068	9.559	0.0004	1.2×10^7
(c)	40	1	1	0.728	8.423	11.427	0.0153	3.7×10^5

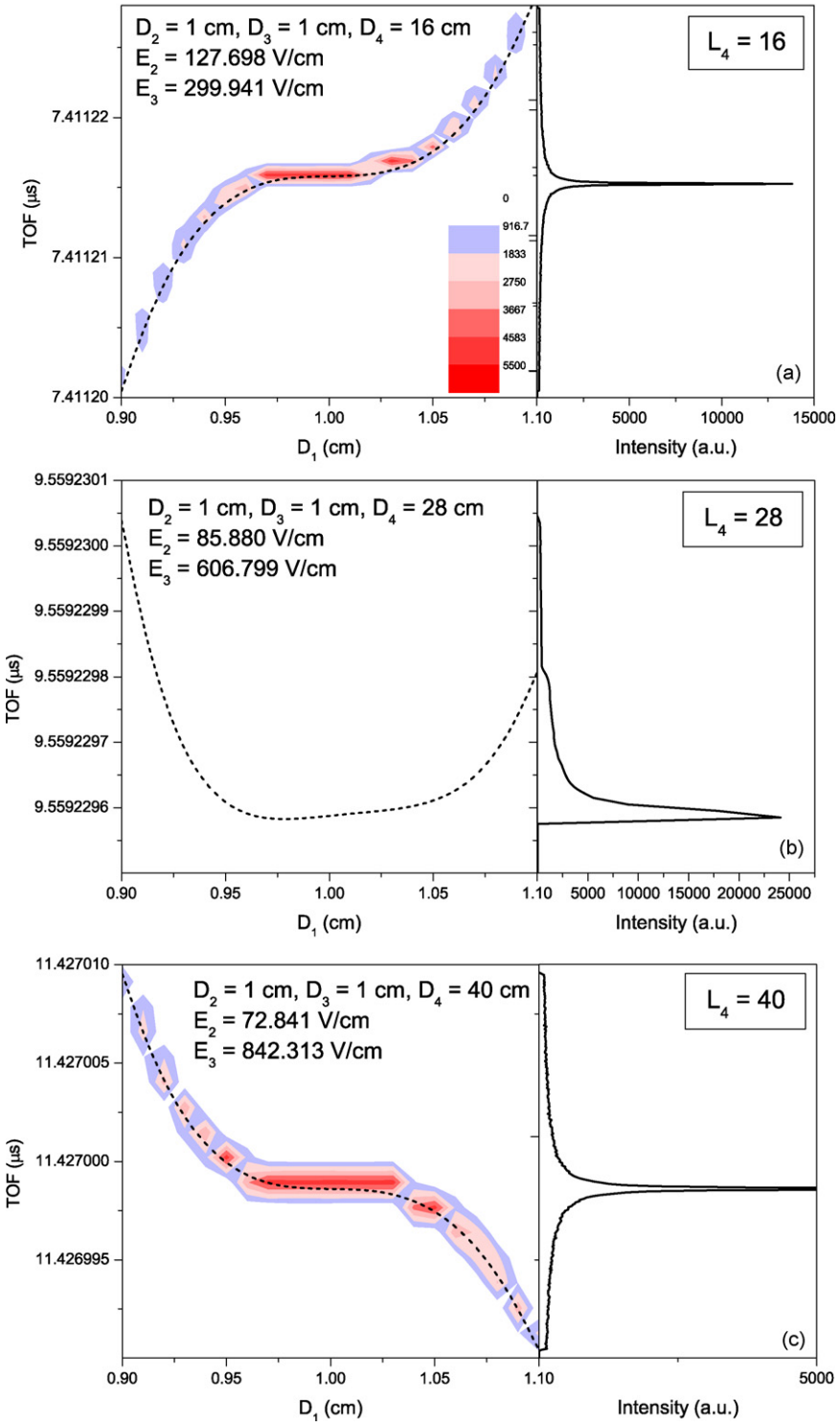

Fig. 9. Flight times distributions as a function of the distance travelled in the ionization region for three three-field TOFMSs with (a) $L_4 = 16$, (b) 28, and (c) 40, for an ion of mass 100 amu and charge +1e. The extraction field is 100.00 V/cm and $\bar{D}_1 = 1$ cm. D_2, D_3, D_4, and E_2 and E_3 are indicated in the figure.

of a third-order space focusing. As expected, $\mathcal{R}_s$ increases with each order of space focus by approximately an order of magnitude.

Fig. 9 shows the simulation of the flight times of ions with 100 and 101 amu originating from different regions for three different values of L_4, 16, 28 and 40. It is seen that the the space resolution for $L_4 = 28$ is better than $L_4 = 40$. The improved resolution is the result of a third-order space focusing. It is seen that the flight time difference due to the initial volume space depend on D_1 (or s), if u_0 is neglected, as a quadratic function for first-order space focusing, a cubic function for second-order focusing, and a fourth-order power function for third-order space focusing. Comparisons of the flight times and resolutions were shown in Table 3. Such designs can provide operational flexibility for higher-order space focusing in a three-field device without increasing the length of the flight tube. Although this is a theoretical improvement of almost two orders of magnitude compared to an optimized two-field TOFMS, it is not realistic to expect this improvement also in practice since a real instrument can probably not be built with the tolerances required.

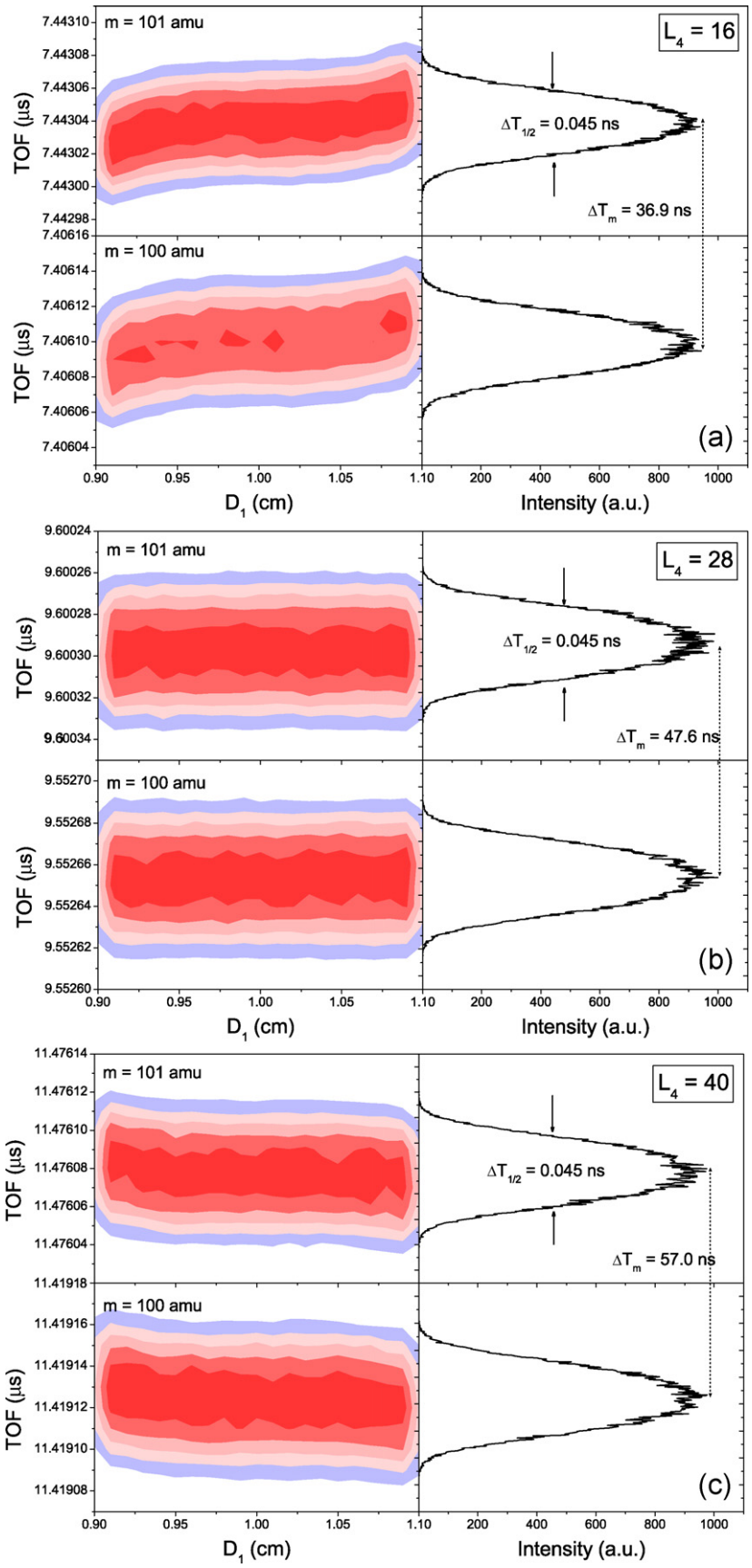

Fig. 10. Simulation of the peaks resulting from ions of mass 100 and 101 amu spread over 0.2 cm wide. Initial velocity was generated according to the beam temperature of 1 mK for three three-field TOFMSs with $L_2 = L_3 = 1$: (a) $L_4 = 16$, (b) 28, and (c) 40.

In addition, thermal energy distributions in a source can not be eliminated with linear TOFMS. For the former, there is a possibility that some compensation of the effect of the machining errors could be made by small modifications to the field strengths in a three-field device, which can optimize focusing.

The simulated time-of-flight spectra for three three-field TOFMSs are shown in Fig. 10 for a beam temperature of 1 mK. It shows that the benefit of third-order space focusing is not clearly seen for 1 mK. The relevant quantities for each three-field case are listed in Table 4.

3.4. Four-field third-order space focusing

Having three independently adjustable electrostatic fields with respect to E_1 allows for a third-order space focusing of the ion packet by the four-field TOFMS, resulting in high space resolution. The difficulty of finding the optimal configuration in a four-field case is solving a large number of parameters like electrode configuration, the distance between them, and voltage ratios, all this in a simple case. During long investigation and modelling of different configurations of four-field TOFMSs, simulations (not shown) showed that the four-field configuration does not provide a significantly improved space resolution compared to three-field cases at a beam temperature of 1 K.

4. A home-made three-field TOFMS

To demonstrate experimentally how the resolution depends on the initial distributions of the ions, we have designed and produced a homemade three-field linear time-of-flight mass spectrometer. The experimental set-up comprised a processing high vacuum chamber, an Nd:YAG laser source with associated beam delivery optics, microchannel plate detector (MCP) and an electronic system for data acquisition and analysis. The laser ionization was produced by laser pulses at 1064 nm using multiphoton ionisation (MPI) schemes, with 6 ns duration (FWHM) at repetition rate of 10 Hz (Continuum Inc.). Ion source and acceleration region assembly consist of stainless steel acceleration plates, each mounted on isolating teflon rod. A 1 m stainless steel field free flight tube is attached to the source chamber which is isolated in vacuum from the flight tube using a 6-in. ultra high vacuum (UHV) gate valve installed between the two components. The source chamber is pumped by a 520 l/s turbomolecular pump (Pfeiffer Vacuum Inc.). Background pressure is typically 10^{-8} mbar, operating vacuum was risen up approximately 10^{-6} mbar and measured using a vacuum gauge. Gas sample introduced into the source chamber by precision UHV leak valve which is designed to control gas admission into high vacuum systems (Caburn-MDC Europe Limited). Ions are detected by using a 40-mm-dual chevron MCP positioned at the end of flight tube (El-Mul Technologies Ldt.). Ion signal is transmitted with 50 Ω impedance collector to a 600 MHz Digital Storage Oscilloscope (LeCroy Corporation), which is triggered by using the output of a fast photodiode (Alphalas GmbH). The laser beam radiation, shaped by passing trough an iris, was focused by a 25 cm focal length lens to a spot size of several micrometers on the ionization region. The size of the laser volume at the focal point has been determined using the formula of $r = 2.44f\lambda/D$ given by several authors (see Refs. [27,28]), where f is focal length of lens used ($f = 25$ cm in this case), λ is the wavelength of laser ($\lambda = 1064$ nm in this paper), and D is the laser diameter just before focusing lens ($D = 0.8$ cm in this case).

D_1 was chosen to be 1.5 cm in our spectrometer. Other lengths were chosen to be $L_2 = 3$, $L_3 = 9$, and $L_4 = 60$, respectively. This configuration gives the best timing resolution in the test runs. The measurements were carried out to determine the resolution of

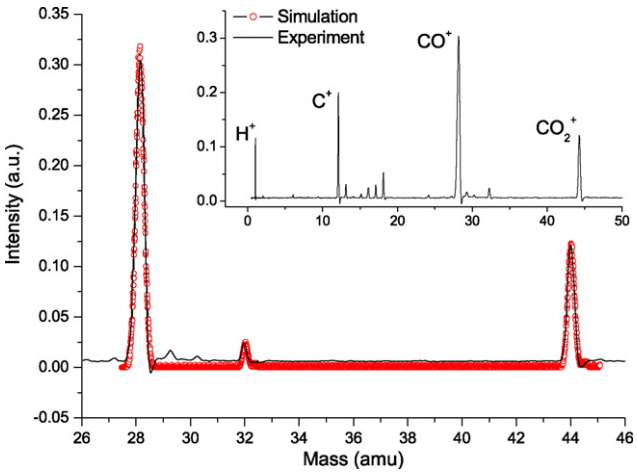

Fig. 11. A typical TOF mass spectrum for CO molecule. Spectrum was obtained at a laser power of 6 W.

the system. A calibration curve to identify different ion peaks in the time-of-flight spectrum has been obtained by plotting a graph between $\sqrt{m/q}$ and the T_m. The typical CO mass spectrum is shown in Fig. 11. From the graph, we obtain a resolution of $m/\Delta m = 200$ at 28 amu. This has been confirmed also by the numerical simulation. At room temperature, the time spread due to the initial velocity distribution is not negligible. Further measurements have been made to see the effects of electric field variations in the extraction and acceleration regions, but the resolution was not significantly changed. This spectrometer is to be used in mass spectroscopic studies in a near future.

5. Conclusion

In this work, an effort has been made to illustrate a systematic approach to the problem of optimizing multi-field TOFMS for space focusing. The second- and third-order space focusing mechanism is theoretically studied and analytical solutions for the given order of space focusing are derived. It is shown that the possibility of third-order focusing in three- or four-field device offers an essential improvement in time resolution. As realized, after the detailed analysis of different configurations, the most flexible and straightforward solution of a high space resolution linear TOFMS is a three-field device. It is therefore important to determine the geometric ratios in such a way that third-order focusing is achieved, especially for the upper limit of the mass of interest. From the simulation with different electrode precision, one can conclude that the manufacturing precision significantly influences the resolution abilities.

When the initial ion velocity u_0 is considered, significant uncompensated time spreads can be produced that limit the mass resolution of the instrument. The results showed that the limitations of the mass resolution by different initial velocities of the ions play a significant role in determining the order of space focusing required in practice. At room temperature no significant improvement in the mass resolution can be expected by increasing the order of space focus, because the time spread due to the velocity dispersion and “turn-around” time of the ion with a mass of 100 amu is about 20 ns. Therefore, the maximum resolving power is about $m/\Delta m = 200$, which is also experimentally measured using a homemade TOFMS.

The effect of velocity dispersion can be minimized by decreasing the amount of time that an ion spends in the ion source, either by increasing the extraction field E_1 or by decreasing the dimensions of the ion source in the direction of ion acceleration (but

not eliminated). Much higher resolution can be obtained by pulsed extraction or by adding a further reflectron stage for energy focusing. Therefore, the best performance of TOF instruments is achieved by a combination of these techniques, and this combination can be the basis for high-performance TOF systems.

Ackowledgements

This work was supported by TUBITAK, through grant 106T679 and 101T192 and Scientific Research Project Coordination Office through grant 2003135 and 05401021 at Selcuk University. The authors would also like to thank Dr. Melike Ulu and Tugbahan Yilmaz for their great help during the development of the apparatus.

References

[1] J. Coles, M. Guilhaus, Orthogonal acceleration—a new direction for time-of-flight mass spectrometry: fast, sensitive mass analysis for continuous ion sources, Trends Anal. Chem. 12 (5) (1993) 203–213.
[2] D. Ioanoviciu, Ion-optical properties of time-of-flight mass spectrometers, Int. J. Mass Spectrom. 206 (2001) 211–229.
[3] B.A. Mamyrin, Time-of-flight mass spectrometry (concepts, achievements, and prospects), Int. J. Mass Spectrom. 206 (2001) 251–266.
[4] M. Guilhaus, Principles and instrumentation in time-of-flight mass spectrometry: physical and instrumental concepts, J. Mass Spectrom. 30 (1995) 1519–1532.
[5] R.J. Cotter, Time-of-Flight Mass Spectrometry, ACS Professional Reference Books, American Chemical Society, 1997.
[6] W.C. Wiley, I.H. McLaren, Time of flight mass spectrometer with improved resolution, Rev. Sci. Instrum. 26 (1955) 1150–1157.
[7] B.A. Mamyrin, V.I. Karataev, D.V. Shmikk, V.A. Zagulin, The mass-reflectron, a new nonmagnetic time-of-flight mass spectrometer with high resolution, Sov. Phys. JETP 37 (1973) 45–51.
[8] W.P. Poschenrieder, Multiple-focusing time-of-flight mass spectrometers. Part II. TOFMS with equal energy acceleration, Int. J. Mass Spectrom. Ion Phys. 9 (1972) 357–373.
[9] T. Sakurai, T. Matsuo, H. Matsuda, Ion optics for time-of-flight mass spectrometers with multiple symmetry, Int. J. Mass Spectrom. Ion Proc. 63 (1985) 273–287.
[10] J.H.J. Dawson, M. Guilhaus, Orthogonal-acceleration time-of-flight mass spectrometer, Rapid Commun. Mass Spectrom. 3 (1989) 155–159.
[11] T. Matsuo, M. Toyoda, T. Sakurai, M. Ishihara, Ion optics for multi-turn time-of-flight mass spectrometers with variable mass resolution, J. Mass Spectrom. 32 (1997) 1179–1185.
[12] J.H.D. Eland, Second-order space focusing in two-field time-of-flight mass spectrometers, Meas. Sci. Technol. 4 (1993) 1522–1524.
[13] F. Chandezon, B. Huber, C. Ristori, A new-regime Wiley–McLaren time-of-flight mass spectrometer, Rev. Sci. Instrum. 65 (11) (1994) 3344–3353.
[14] P. Piseri, S. Iannotta, P. Milani, Parameterization of a two-stage mass spectrometer performing second-order space focusing, Int. J. Mass Spectrom. Ion. Proc. 153 (1996) 23–28.
[15] U. Even, B. Dick, Computer optimization for high-resolution time-of-flight mass spectrometer, Rev. Sci. Instrum. 71 (2000) 4415–4420.
[16] U. Even, B. Dick, Optimization of a one-dimensional time-of-flight mass spectrometer, Rev. Sci. Instrum. 71 (2000) 4421–4430.
[17] D.P. Seccombe, T.J. Reddish, Theoretical study of space focusing in linear time-of-flight mass spectrometers, Rev. Sci. Instrum. 72 (2001) 1330–1338.
[18] SIMION 3D v8.0, Scientific Instrument Services, Inc. http://www.simion.com.
[19] R. Antoine, L. Arnaud, M. Abd El Rahim, D. Rayane, M. Broyer, Ph. Dugourd, Distortion of ion trajectories in a time-of-flight mass spectrometer: simulations and experiments with a position sensitive detector, Int. J. Mass Spectrom. 239 (2004) 1–6.
[20] U. Rohner, J.A. Whitby, P. Wurz, S. Barabash, Highly miniaturized laser ablation time-of-flight mass spectrometer for a planetary rover, Rev. Sci. Instrum. 75 (2004) 1314–1322.
[21] A.D. Appelhans, J.E. Delmore, J.E. Olson, Wide dispersion multiple collector isotope ratio mass spectrometer, Int. J. Mass Spectrom. 241 (2005) 1–9.
[22] L. Sarkadi, A. Orbán, A time-of-flight electron spectrometer for studies of forward electron emission in ion–atom collisions, Meas. Sci. Technol. 17 (2006) 84–90.
[23] D. Papanastasiou, A.W. McMahon, Correlated phase space distributions of ions in an orthogonal time-of-flight mass spectrometer, Int. J. Mass Spectrom. 254 (2006) 20–27.
[24] L.H. Coutinho, G. Tosin, P.T. Fonseca, R.L. Cavasso-Filho, F.C. Cruz, A. Naves de Brito, A time-of-flight spectrometer for synchrotron radiation-based recoil ion momentum spectroscopy in laser cooled atoms, Nucl. Instrum. Methods Phys. Res. A 571 (2007) 748–754.
[25] T.J.M. Zouros, O. Sise, F.M. Spiegelhalder, D.J. Manura, Investigation of the accuracy of ion optics simulations using Kepler orbits in a spherical capacitor, Int. J. Mass Spectrom. 261 (2007) 115–133.
[26] D.A. Dahl, T.R. McJunkin, J.R. Scott, Comparison of ion trajectories in vacuum and viscous environments using SIMION: insights for instrument design, Int. J. Mass Spectrom. 266 (2007) 156–165.
[27] A.J. Langley, W.J. Noad, I.N. Ross, W. Shaikh, High-brightness femtosecond laser using titanium–sapphire technology and amplification in dyes, Appl. Opt. 33 (1994) 3875–3880.
[28] H.S. Kilic, K.W.D. Ledingham, C. Kosmidis, T. McCanny, R.P. Singhal, S.L. Wang, D.J. Smith, A.J. Langley, W. Shaikh, Multiphoton ionization and dissociation of nitromethane using femtosecond laser pulses at 375 and 750 nm, J. Phys. Chem. A 101 (1997) 817–823.